

Loading uniform Ag_3PO_4 nanoparticles on three-dimensional peony-like WO_3 for good stability and excellent selectivity towards NH_3 at room temperature

Xingyan Shao(邵星炎), Fuchao Jia(贾福超), Tingting Liu(刘婷婷), Jiancheng Liu(刘健诚), Xiaomei Wang(王小梅), Guangchao Yin(尹广超), Na Lv(吕娜), Tong Zhou(周通), Ramachandran Rajan, and Bo Liu(刘波)

Citation: Chin. Phys. B, 2023, 32 (**8**): 080703. DOI: 10.1088/1674-1056/ac98a0
Journal homepage: http://cpb.iphy.ac.cn; http://iopscience.iop.org/cpb

What follows is a list of articles you may be interested in

Loading uniform Ag_3PO_4 nanoparticles on three-dimensional peony-like WO_3 for good stability and excellent selectivity towards NH_3 at room temperature

Xingyan Shao(邵星炎), Fuchao Jia(贾福超), Tingting Liu(刘婷婷), Jiancheng Liu(刘健诚), Xiaomei Wang(王小梅), Guangchao Yin(尹广超), Na Lv(吕娜), Tong Zhou(周通), Ramachandran Rajan, and Bo Liu(刘波)
Chin. Phys. B, 2023, 32 (**8**): 080703. DOI: 10.1088/1674-1056/ac98a0

A self-powered and sensitive terahertz photodetection based on $PdSe_2$

Jie Zhou(周洁), Xueyan Wang(王雪妍), Zhiqingzi Chen(陈支庆子), Libo Zhang(张力波), Chenyu Yao(姚晨禹), Weijie Du(杜伟杰), Jiazhen Zhang(张家振), Huaizhong Xing(邢怀中), Nanxin Fu(付南新), Gang Chen(陈刚), and Lin Wang(王林)
Chin. Phys. B, 2022, 31 (**5**): 050701. DOI: 10.1088/1674-1056/ac4908

Copper ion beam emission in solid electrolyte $Rb_4Cu_{16}I_{6.5}Cl_{13.5}$

Tushagu Abudouwufu(吐沙姑·阿不都吾甫), Xiangyu Zhang (张翔宇), Wenbin Zuo (左文彬), Jinbao Luo(罗进宝), Yueqiang Lan(兰越强), Canxin Tian (田灿鑫), Changwei Zou(邹长伟), Alexander Tolstoguzov, and Dejun Fu(付德君)
Chin. Phys. B, 2022, 31 (**4**): 040704. DOI: 10.1088/1674-1056/ac2f31

Highly-sensitive NO, NO_2, and NH_3 measurements with an open-multipass cell based on mid-infrared wavelength modulation spectroscopy

Xiang Chen(陈祥), Chen-Guang Yang(杨晨光), Mai Hu(胡迈), Jian-Kang Shen(沈建康), Er-Chao Niu(牛二超), Zhen-Yu Xu(许振宇), Xue-Li Fan(范雪丽), Min Wei(魏敏), Lu Yao(姚路), Ya-Bai He(何亚柏), Jian-Guo Liu(刘建国), Rui-Feng Kan(阚瑞峰)
Chin. Phys. B, 2018, 27 (**4**): 040701. DOI: 10.1088/1674-1056/27/4/040701

Crystal structure and thermochemical properties of phase change materials bis(1-octylammonium) tetrachlorochromate

Lu Dong-Fei (卢冬飞), Di You-Ying (邸友莹), He Dong-Hua (何东华)
Chin. Phys. B, 2012, 21 (**8**): 080702. DOI: 10.1088/1674-1056/21/8/080702

Loading uniform Ag_3PO_4 nanoparticles on three-dimensional peony-like WO_3 for good stability and excellent selectivity towards NH_3 at room temperature

Xingyan Shao(邵星炎)[1,2], Fuchao Jia(贾福超)[1,†], Tingting Liu(刘婷婷)[1,2], Jiancheng Liu(刘健诚)[1], Xiaomei Wang(王小梅)[1], Guangchao Yin(尹广超)[1], Na Lv(吕娜)[3], Tong Zhou(周通)[1], Ramachandran Rajan[1,4], and Bo Liu(刘波)[1,2,‡]

[1] *Laboratory of Functional Molecules and Materials, School of Physics and Optoelectronic Engineering, Shandong University of Technology, Zibo* 255000, *China*

[2] *School of Material Science and Engineering, Shandong University of Technology, Zibo* 255000, *China*

[3] *Provincial Key Laboratory of Network Based Intelligent Computing, University of Jinan, Jinan* 250022, *China*

[4] *Translational Medical Center, Zibo Central Hospital, Zibo* 255036, *China*

(Received 20 May 2022; revised manuscript received 5 October 2022; accepted manuscript online 10 October 2022)

A heterojunction structure design is a very good method for improving the properties of semiconductors in many research fields. This method is employed in the present study to promote the gas-sensing performance of Ag_3PO_4 nanocomposites at room temperature (25 °C). A nanocomposite of Ag_3PO_4 nanoparticles and three-dimensional peony-like WO_3 (WO_3/Ag_3PO_4) was successfully prepared by the precipitation method. The crystalline phases were analyzed by x-ray diffraction and the microstructure was characterized by scanning electron microscopy and transmission electron microscopy. The chemical bonding states were analyzed by x-ray photoelectron spectroscopy. The gas-sensing performance of WO_3/Ag_3PO_4 sensors was systematically explored at room temperature. The composite sensors possessed a higher response and lower detection limit (1 ppm) to NH_3 than those made of a single type of material; this is ascribed to the synergistic effect achieved by the heterojunction structure. Among the different composite sensors tested, gas sensor A5W5 (Ag_3PO_4:WO_3 mass ratio of 5:5) displayed the highest response to NH_3 at room temperature. Interestingly, the A5W5 gas sensor exhibited relatively good stability and excellent selectivity to NH_3. The A5W5 sensor also displayed a relatively good response under high humidity. The gas-sensing mechanism of the WO_3/Ag_3PO_4 sensors is explained in detail. Taken together, the as-prepared sensor is highly efficient at detecting NH_3 and could be suitable for practical applications. In addition, this study also provides a new method for developing Ag_3PO_4-based sensors in the gas-sensing field.

Keywords: Ag_3PO_4, peony-like WO_3, NH_3, room temperature

PACS: 07.07.Df **DOI:** 10.1088/1674-1056/ac98a0

1. Introduction

The atmospheric environment has been severely polluted by a large number of toxic and pungent gases due to the rapid development of various industries and technologies. Among these gases, ammonia (NH_3), a colorless gas with a pungent odor, is highly toxic and can cause great harm to humans, for example eye irritation and burning of the nose and throat, and in extreme cases may result in respiratory failure. The American Conference of Governmental Industrial Hygienists reported that the threshold limit value for NH_3 exposure is 25 ppm.[1,2] Ammonia is not only a building block for the synthesis of many pharmaceuticals but is also used in cleaning products.[1] Hence, it is essential to fabricate a gas sensor with high stability, selectivity and sensitivity for the fast detection of NH_3.

With the rapid and nonstop development of the semiconductor industry, SnO_2,[3–6] ZnO [7–10] and TiO_2 [11–14] have often been used to detect NH_3 due to their excellent chemical and thermal stability, high electron mobility, adjustable electron state and quantum constraint.[15,16] Despite these merits, the practical applications of semiconductor materials are limited because of their high operating temperature and poor selectivity to NH_3, which greatly shortens the lifetime of devices and usage in real life.[17–19] This has encouraged researchers to search for new kinds of gas-sensing materials for the detection of NH_3 at low or room temperatures. For instance, several works have separately employed P-doped graphene, RGO/3-CuPc and fluorinated graphene oxide to detect NH_3 at room temperature.[2,20,21] However, most of these materials had a common disadvantage in that the response to NH_3 was very weak. Hence, there is an urgent need to improve the response of nanomaterials to NH_3 at room temperature. Recently, Zhang and co-workers reported that Ag_3PO_4 nanoparticles not only displayed a higher response to NH_3 at nearly 50 °C than at other test temperatures but also had excellent selectivity.[22] However, the long-term stability of Ag_3PO_4-based gas sensors was found to be very poor under natural light

†Corresponding author. E-mail: jiafuchao@sdut.edu.cn
‡Corresponding author. E-mail: liub@sdut.edu.cn

© 2023 Chinese Physical Society and IOP Publishing Ltd

because Ag^+ present in Ag_3PO_4 nanoparticles was reduced to silver metal by gaining electrons from light energy, thus hindering real-life applications. Therefore, it is of paramount importance to improve the stability of Ag_3PO_4 nanoparticles for gas-sensing applications.

In order to obtain a NH_3 gas sensor with excellent selectivity and stability at room temperature, a sensor made from WO_3 decorated with Ag_3PO_4 nanoparticles was designed according to energy band theory. When two n-type semiconductors come into contact with each other, the electrons transfer from the conduction band of the semiconductor with the higher Fermi level (Ag_3PO_4) to the semiconductor with a lower Fermi level (WO_3) until the Fermi level reaches equilibrium; this can dramatically enhance the stability of a Ag_3PO_4-based gas sensor and effectively enhance the separation of electron–hole pairs. At the same time, the utilization rate of electrons is also promoted, leading to an increased concentration of oxygen species (O_2^- O^-, O^{2-}) because the adsorbed oxygen molecules on semiconductor surfaces can capture more electrons from the conduction band. This can remarkably improve the gas-sensing properties of the semiconductor. The composite gas sensor still has outstanding selectivity to NH_3 due to the presence of Ag_3PO_4 nanoparticles.

Herein, a composite of Ag_3PO_4 and three-dimensional (3D) peony-like WO_3 with different mass ratios was synthesized through a precipitation method. The gas-sensing performance of Ag_3PO_4/WO_3 sensors was systematically explored and compared with pristine WO_3 and Ag_3PO_4. Interestingly, the as-prepared composite showed a better response and lower detection limit to NH_3 than the pure materials. The gas sensor possessed relatively good stability, which greatly enhanced the utility of Ag_3PO_4 nanoparticles in the gas-sensing field. Finally, we discuss the mechanism of gas sensing in detail.

2. Experimental details

2.1. Chemicals

Sodium tungstate (Na_2WO_4), sodium sulfate (Na_2SO_4), disodium hydrogen phosphate (Na_2HPO_4), sodium phosphate ($Na_3PO_4{\cdot}12H_2O$), dimethyl sulfoxide (DMSO), silver nitrate ($AgNO_3$) and ethanol were purchased from Sinopharm Chemical Reagent Co. Ltd, China. These chemicals were used in the experiment without further purification.

2.2. Preparation of 3D peony-like WO_3

Three-dimensional peony-like WO_3 was synthesized according to the literature.[23] Firstly, 239.8 mg of Na_2WO_4 was dissolved in 20 ml of deionized water under constant magnetic stirring. Secondly, as-prepared Na_2WO_4 solution was added dropwise to a suspension containing 40 g of Na_2SO_4, 5 ml of condensed hydrochloric acid (HCl; 37 wt%, 12 $mol{\cdot}l^{-1}$) and 15 ml of water. The suspension was stirred for 3 h and then transferred into a teflon-lined stainless steel autoclave with a capacity of 100 ml. The autoclave was then sealed and hydrothermally treated at 200 °C for 10 h. Finally, white powders of 3D peony-like WO_3 were obtained by centrifugation (7000 rpm) and drying (60 °C, 10 h).

2.3. Preparation of Ag_3PO_4/WO_3 composite

WO_3/Ag_3PO_4 composite was synthesized by a precipitation method.[24] The typical synthesis procedure can be described as follows. Firstly, a certain amount of $AgNO_3$ was added to a mixture solution containing deionized water (12.5 ml) and DMSO (25 ml) under constant stirring. A certain amount of WO_3 was dispersed into the mixture solution under continuous stirring for 15 min, followed by the dropping of Na_2HPO_4 aqueous solution (0.15 M) (Fig. 1). Table 1 lists the composition of various reaction solutions prepared in this study. After stirring for 30 min, the obtained precipitate was collected by centrifugation, washed with ethanol and deionized water several times, and dried at 60 ° for 10 h. According to the mass ratio of Ag_3PO_4 to WO_3, the prepared composite materials were denoted as A3W7, A5W5 and A7W3.

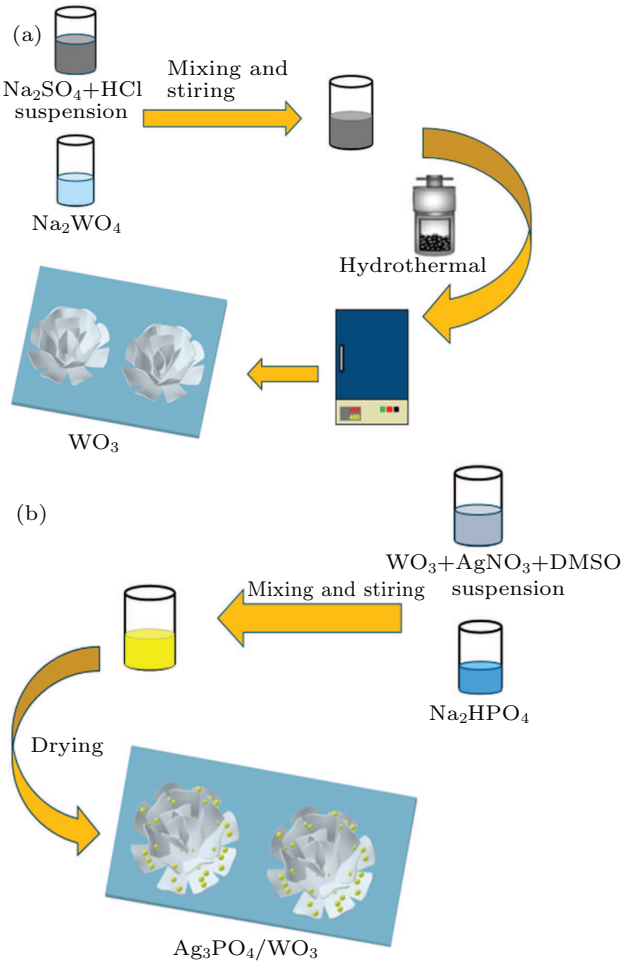


Fig. 1. (a) The synthesis process for peony-like WO_3. (b) The synthesis process for Ag_3PO_4/WO_3.

Table 1. The synthesis conditions of Ag_3PO_4/WO_3.

Sample	Mass ratio (Ag_3PO_4:WO_3)	Amount of $AgNO_3$ (g)	Amount of WO_3 (g)	Volume of Na_2HPO_4 solution (ml)
A3W7	3:7	0.06	0.064	3.0
A5W5	5:5	0.10	0.046	5.0
A7W3	7:3	0.14	0.027	7.0

2.4. Characterization

The phases of the as-prepared samples were analyzed by x-ray diffraction (XRD; Bruker D8 Advance A25) in the range of 5°–80° with a scanning rate of 10°·min^{-1}. The morphology and microstructure were obtained via using scanning electron microscopy (SEM; Quanta 250) and transmission electron microscopy (TEM; FEI Tecnai G2F 20, USA). The chemical elements and their valence states were characterized by x-ray photoelectron spectroscopy (XPS) with an Al K_α (1486.6 eV) anode (Thermo Fisher Scientific Thermo ESCALAB 250Xi, USA).

2.5. Sensor fabrication and measurements

The sample was ground in a mortar using anhydrous ethanol and then brushed onto the ceramic tube. There were two gold electrodes at both ends of the ceramic tube and these were connected with two Pt wires on each electrode. The sensor was heated by the Ni–Cr wire present in the middle of the ceramic tube and six wires were welded onto the black base (Fig. 2(a)). The black base was stuck on the support circuit board (Fig. 2(b)) and then placed on an aging table for 5 days at 100 °C. Finally, the support circuit board was stuck on the testing system and the test was connected to the computer in order to obtain the data (Figs. 2(c) and 2(d)). A circuit diagram of the gas-sensing test system is shown in Fig. 2(e). The whole test was performed in a darkroom. The response was defined as $S = R_a/R_g$, where R_a is the resistance of the gas sensor in the air and R_g is the resistance of the gas sensor in the test gas. The temperature of the test environment was maintained at 25 °C with an air conditioner. The relative humidity (RH) of the test chamber was consistent with the laboratory environment. The RH of the environment was generally maintained at about 40%–50%. If the RH of the test chamber needed to be increased, water was injected onto the heating plate in the test chamber by a micro-injector. The RH sensor in the test chamber directly displayed the RH value from the computer. When the RH reached the test requirement, the gas-sensing measurements were performed.

3. Results and discussion

3.1. Characterization

XRD was employed to identify the crystal structure and phase composition of WO_3 and Ag_3PO_4 as well as the composites of both. The results are shown in Fig. 3. For virgin WO_3, the characteristic diffraction peaks located at 13.9°, 22.8°, 24.3°, 26.8°, 28.0°, 33.6°, 36.5°, 42.7°, 44.3°, 46.6°, 49.7°, 55.3°, 58.0°, 63.2° and 70.5° corresponded to (100), (001), (110), (101), (200), (111), (201), (300), (211), (002), (220), (202), (400), (401) and (222) crystal planes, respectively. These data were indexed to the hexagonal structure of WO_3 (JCPDS No. 81-0577). The spectrum of pure Ag_3PO_4 exhibited peaks at 21.7°, 29.7°, 33.3°, 36.5°, 47.8°, 52.6°, 54.9°, 57.2° and 61.6°, corresponding to (110), (200), (210), (211), (310), (222), (320), (321) and (400) crystal planes, respectively. These data were well matched with the body-centered cubic structure of Ag_3PO_4 (JCPDS No. 06-0505). In the case of composite materials, the intensity of the Ag_3PO_4 diffraction peaks was evidently increased with increasing mass ratio of Ag_3PO_4:WO_3 from 3:7 to 7:3, while the intensities of the WO_3 diffraction peaks gradually declined. No extra diffraction peaks were observed in the composite. Thus, these two kinds of material were physically complex together. Finally, there was no additional diffraction peak for impurities, indicating high purity and good crystallinity of the prepared sample.

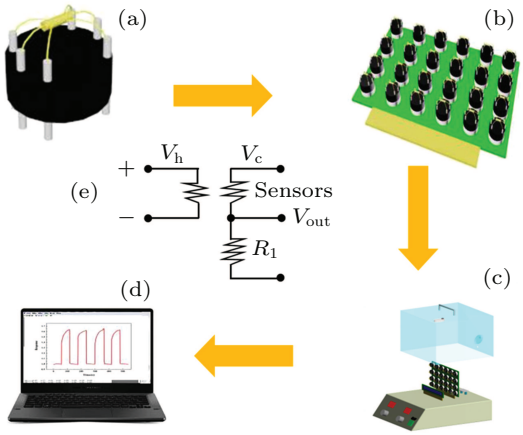


Fig. 2. (a) The gas sensor. (b) The support circuit board. (c) The gas-sensing test system. (d) Software for the gas-sensing test. (e) Circuit diagram of gas-sensing test system.

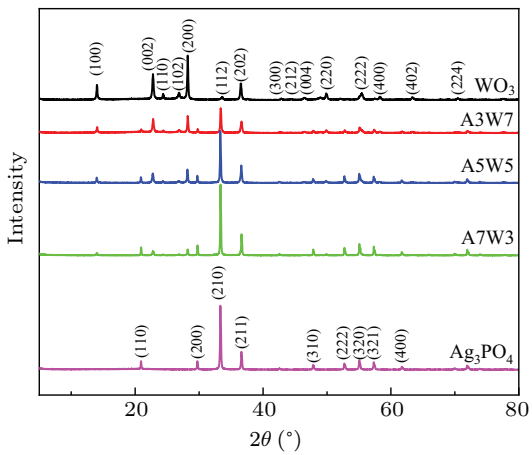


Fig. 3. XRD patterns of the as-prepared samples.

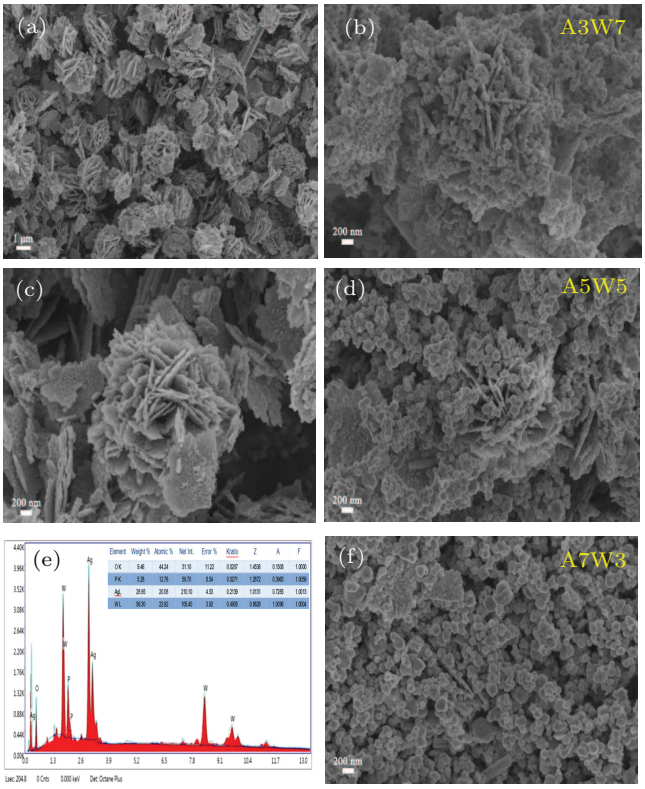


Fig. 4. (a), (b) SEM images of WO_3. (c) SEM image of A3W7. (d) SEM image of A5W5. (e) Energy dispersive x-ray analysis of A5W5. (f) SEM image of A7W3.

The morphology of nanomaterials significantly influenced the process of gas adsorption and desorption. SEM was used to characterize the morphology of the materials, and the results are displayed in Fig. 4. The 3D peony-like WO_3 assembled from nanosheets of WO_3 can be clearly seen (Fig. 4(a)). This type of material possesses a high surface area, which in turn can improve the gas-sensing performance of the sensor. The 3D peony-like structure provides excellent stable support for the loading of Ag_3PO_4 nanoparticles (Fig. 4(c)). Figures 4(b), 4(d) and 4(f) describe the differences in the morphology of the composites with respect to changes in the mass ratio from 3:7 to 7:3 (A3W7, A5W5 and A7W3). These SEM images demonstrate that the 3D peony-like WO_3 is gradually covered by uniform Ag_3PO_4 nanoparticles with increase in the mass ratio. Thus, these two materials are sufficiently in contact with each other, which benefits electron transfer between the two semiconductor materials due to the difference in their Fermi levels, ultimately leading to enhancement of the gas-sensing property of the composite. The energy dispersive x-ray analysis result for A5W5 is depicted in Fig. 4(e). It is obvious that each element was allocated in the expected proportions. In addition, the grain size distribution of Ag_3PO_4 nanoparticles was counted and is shown in Fig. S2. The statistical results reveal that the diameter of these nanoparticles ranged from 100 nm to 140 nm. The grain size of Ag_3PO_4 nanoparticles in this study was relatively smaller than in previous studies.[25,26] Finally, the 3D peony-like morphology of the composite was also explored by SEM after scraping the composite of the ceramic tube after the gas-sensing test; the result is shown in Fig. S1. It is clear that there is no variation in the morphology for single materials and the composite, which guarantees the reliability of the gas-sensing measurements.

The fine structural characteristics of composite A5W5 were further investigated by TEM analysis, as shown in Fig. 5. The low-magnification image (Fig. 5(a)) clearly shows the 3D peony-like structure of A5W5, which well matches the SEM result. The high-magnification image (Fig. 5(b)) displays distinct lattice fringes of Ag_3PO_4 and WO_3. The space between the two adjacent lattice planes of Ag_3PO_4 and WO_3 was 0.252 nm and 0.384 nm, corresponding to the (211) plane of cubic Ag_3PO_4[27] and the (001) plane of hexagonal WO_3,[28] respectively. For the Ag_3PO_4/WO_3 nanocomposite, abundant trap states were obtained at the grain boundaries and deep defects at the interface, which can be beneficial to the gas adsorption and charge transfer processes of the electronic sensor, leading to enhancement of the gas-sensing performance.[29] The elemental mapping results are shown in Figs. 5(c)–5(f). The distribution of each element was found to be relatively uniform and no impurities were observed.

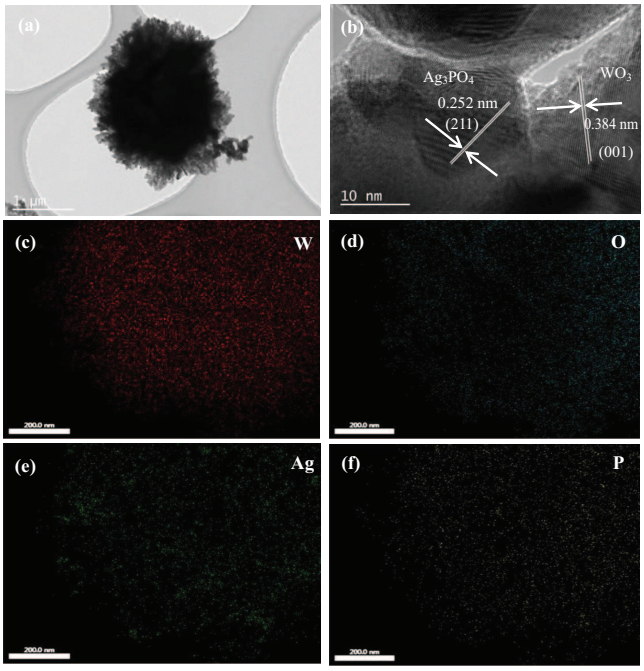


Fig. 5. (a), (b) TEM images of A5W5. (c)–(f) Elemental mapping images of W, O, Ag and P.

In order to confirm the chemical bonding states of different elements, XPS analysis was carried out; the spectra are shown in Fig. 6. The two peaks situated at 368.03 eV and 374.04 eV were ascribed to the Ag^+ $3d_{5/2}$ and $3d_{3/2}$ binding energies, respectively, found in Ag_3PO_4 (Fig. 6(a)).[30] The peak for metallic silver was not observed in the Ag 3d spectrum of Ag_3PO_4, implying that Ag_3PO_4 in A5W5 was not

degraded owing to the formation of a Ag_3PO_4/WO_3 heterojunction, and the aim of improving the stability of Ag_3PO_4 was indeed achieved. Figure 6(b) shows the W 4f XPS spectrum of A5W5 in which spin–orbit doublets corresponding to W $4f_{7/2}$ and W $4f_{5/2}$ peaks were observed at 35.76 eV and 37.9 eV, respectively; the difference in the binding energy between W$4f_{7/2}$ and W $4f_{5/2}$ is 2.14 eV, indicating a normal state of W^{6+} in sample A5W5. These values were well matched with those reported in the literature.[31] The P 2p high-resolution spectrum is shown in Fig. 6(c). The two peaks located at 132.35 eV and 133.19 eV are ascribed to the binding energy of $2p_{3/2}$ and $2p_{1/2}$, respectively, of P^{5+} in Ag_3PO_4 in sample A5W5.[25] For O 1s (Fig. 6(d)), the peak observed at 530.6 eV is assigned to the crystal lattice oxygen while the peak at 532.0 eV is related to the adsorbed oxygen.[26] Thus, XPS analysis corroborates the formation of Ag_3PO_4/WO_3 composite.

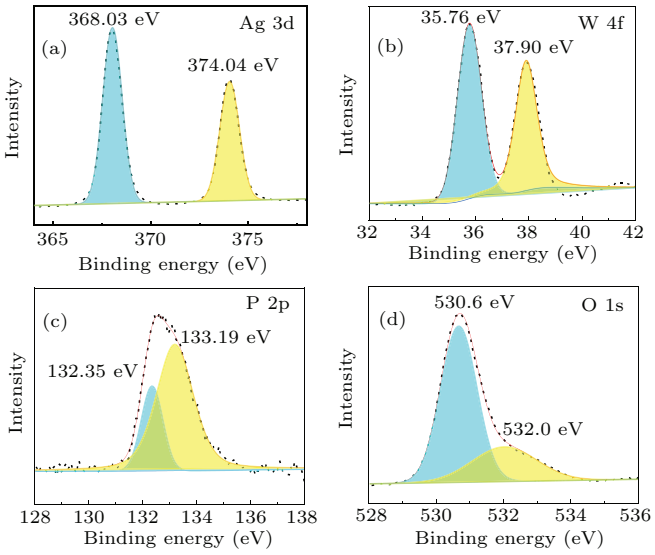


Fig. 6. (a)–(d) XPS survey spectrum of Ag 3d, W 4f, P 2p and O 1s, respectively.

3.2. Gas-sensing measurements

The gas-sensing performance of these sensors for NH_3 was systematically measured, and the results are shown in Figs. 7(a)–7(d). At first, the gas-sensing responses to NH_3 were detected by WO_3, A3W7, A5W5, A7W3 and Ag_3PO_4. The test results are displayed in Fig. 7(a). It is obvious from these results that the A5W5 gas sensor had the highest response to NH_3 compared with the other sensors tested in this study. It was worth noting that the low detection limit of the composite was 1 ppm, which was much lower than with pure WO_3 and Ag_3PO_4 sensors. The acceptable linear tendency for the A5W5 gas sensor to NH_3 ranged from 1 ppm to 20 ppm, as shown in the inset of Fig. 7(b). Therefore, this sensor could be very useful for early warning of NH_3 leakage. The short-term stability of WO_3 sensors and composites to 100 ppm NH_3 was then tested and the results are presented in Fig. 7(c). The measurement results show that the as-prepared sensors have good short-term stability after four consecutive cycles of testing. The long-term stability of a gas sensor is one of the most important factors for judging the quality of the sensor. Therefore, the long-term stability of the A5W5 sensor was tested, and the results showed that the fluctuation in response was slight over 5 weeks, proving that the A5W5 sensor has better long-term stability (Fig. 7(d)) than a pristine Ag_3PO_4 sensor.[22] Thus, the stability of a Ag_3PO_4 sensor is remarkably improved by efficient complexing with semiconductor materials.

For real-life applications of gas sensors, the influence on the sensors of RH in the background environment should be estimated at room temperature. Hence, the effect of RH on the performance of the A5W5 gas sensor was explored and the results are shown in Fig. 8. Figure 8(a) displays the response of an A5W5 gas sensor to 100 ppm NH_3 at different levels of humidity at room temperature. In this study, the response value of the sensor was decreased with increase in RH, which could be ascribed to the absorption reaction and the Grothuss chain reaction of water molecules on the surface of the gas sensor.[12] The Grothuss chain reaction is the reaction of H_3O^+ and H_2O on the serial water layer; the reaction equation is as follows:[12]

$$H_2O+H_3O^+ \rightarrow H_3O^+ + H_2O.$$

Actually, this process is always accompanied by the transfer of charge. When H_3O^+ ions release a proton to the neighboring water molecules, this proton is accepted while another proton is released, and so on. Thus, when RH is maintained at a relatively low level there are not enough water molecules to form a continuous water layer on the surface of the gas sensor. Many oxygen absorption sites are still exposed, and the oxygen molecules on the absorption sites capture electrons from the conduction band of the composites, creating an electron depletion layer; this results in the conduction channel of electrons becoming narrower and the gas sensor has high resistance. Still, the sensor showed good gas-sensing performance to NH_3. As the RH increases, the absorption sites are occupied by the continuous water layer. Hence, the number of oxygen species decreases, the width of the electron depletion layer becomes narrower and the resistance of the gas sensor decreases (as shown in the inset of Fig. 8(a)), which would, in turn, decrease the sensitivity of the gas sensor. The evolution of the resistance and the RH was fitted to a curve, enabling us to figure out the approximate resistance of the sensor based on humidity (inset of Fig. 8(a)). Figure 8(b) shows the decreasing response of the A5W5 gas sensor to 100 ppm NH_3 under different RHs at room temperature. These results suggest that there is a negligible effect on the gas-sensing response of the sensor when the RH is lower than 54%. However, when the

RH exceeds 76%, the response of the gas sensor to NH_3 declines remarkably, probably due to the formation of a continuous water layer. Although the number of oxygen absorption sites is decreased, the A5W5 sensor still shows a relatively good response under high humidity, conducive to the detection of NH_3 under extreme environmental conditions.[12]

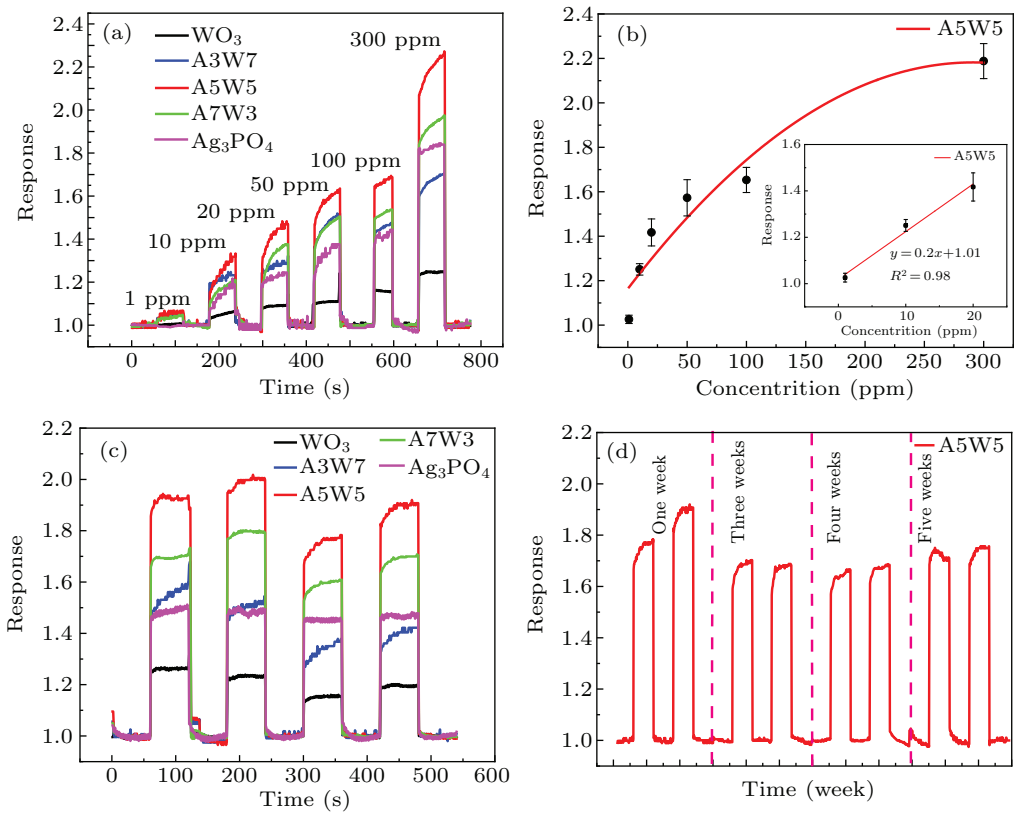


Fig. 7. (a) The dynamic response values of different gas sensors to NH_3. (b) The response of the A5W5 sensor to different concentrations of NH_3. (c) Short-term stability of different sensors to 100 ppm NH_3. (d) Long-term stability of the A5W5 sensor to 100 ppm NH_3.

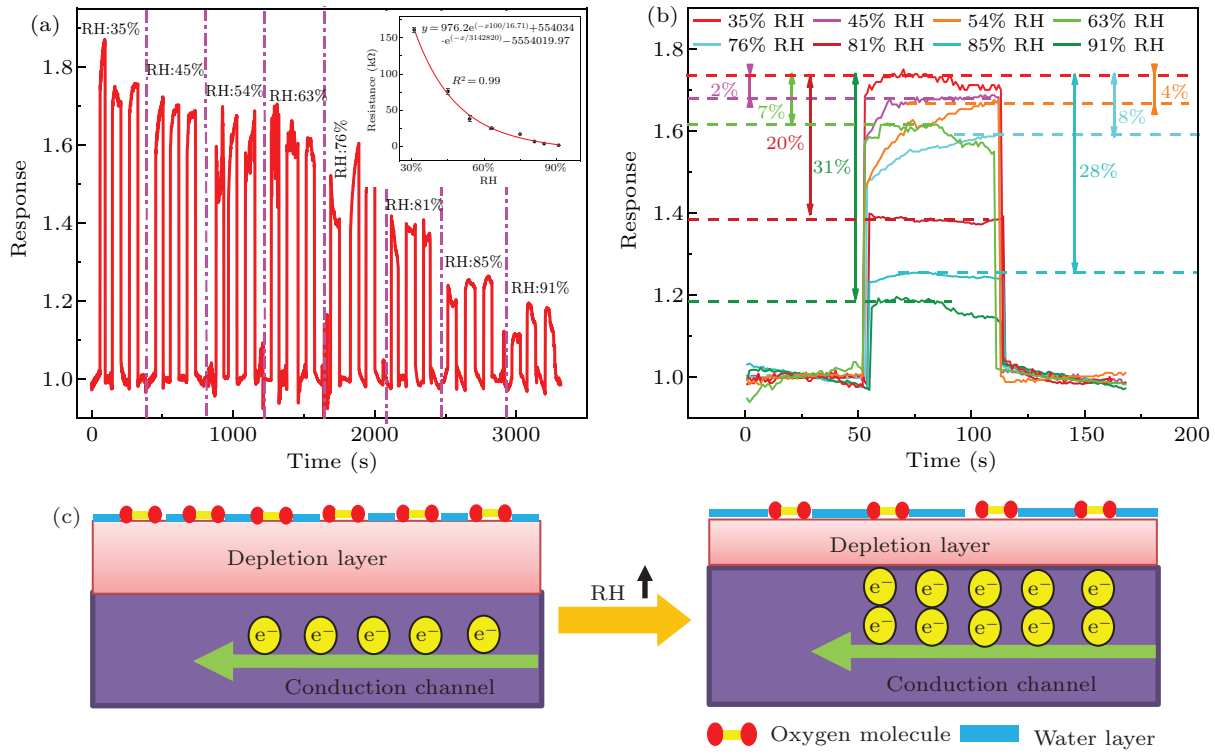


Fig. 8. (a) The evolution of response value and the resistance (inset) of the A5W5 gas sensor to 100 ppm NH_3 under different RHs at room temperature. (b) The relative decrease in the response value of the A5W5 gas sensor to 100 ppm NH_3 under different RHs at room temperature. (c) Schematic of the Grothuss chain reaction.

Selectivity is one of the most important characteristic features of gas sensors for practical applications. Firstly, the response of the A5W5 sensor to acetone, ethanol, methanol, isopropanol and ammonia (the target gas concentration was 100 ppm) was separately measured at room temperature. As shown in Fig. 9(a), the response of the A5W5 sensor to NH_3 was remarkably higher than to the other gases tested. Secondly, the responses of the sensor were analyzed after mixing NH_3 with other kinds of gases. As depicted in Fig. 9(b), the gas-sensing performance of the A5W5 sensor to NH_3 was not affected even after mixing it with other gas molecules. Thirdly, four other gases were first injected into the gas cavity, then NH_3 was injected (Fig. 9(c)). Although the response value was slightly lower than in the previous situation, the A5W5 sensor still exhibited a higher response to NH_3. These results indicate that the A5W5 gas sensor possesses excellent selectivity to NH_3. The reason for the high selectivity of the A5W5 gas sensor to NH_3 can be explained as follows. NH_3 molecules with a lone pair of electrons could tend to organize the bare orbitals of silver atoms, while the oxygen atoms present on Ag_3PO_4 also had a lone pair of electrons and could form hydrogen bonds with the hydrogen atoms of NH_3.[22]

Finally, gas-sensing performance of the Ag_3PO_4/WO_3 gas sensor to NH_3 compared with previously reported sensors is summarized in Table 2. Interestingly, our sensor surpassed most of the reported sensors in terms of response at room temperature.

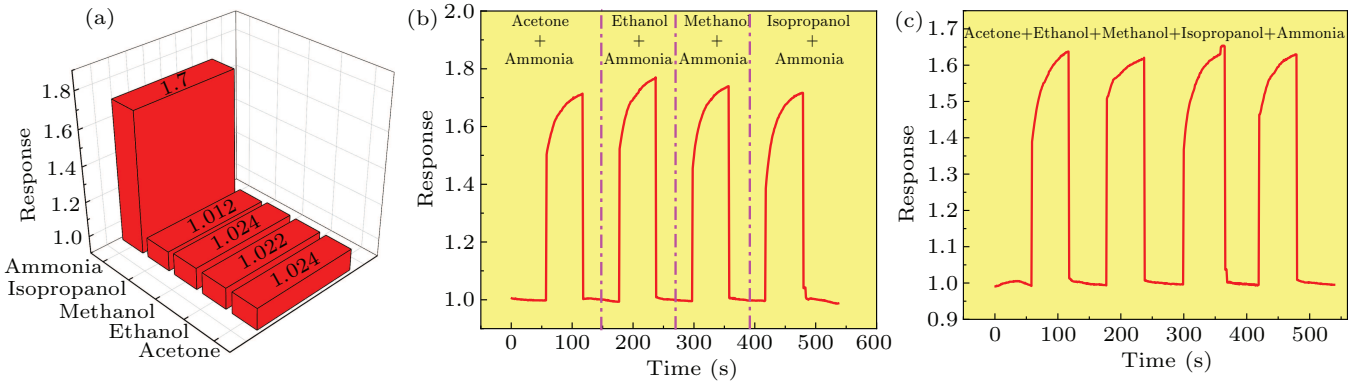


Fig. 9. (a) The response of the A5W5 gas sensor to different target gases. (b) The response of the A5W5 gas sensor to two mixed target gases. (c) The response of the A5W5 gas sensor to five mixed target gases.

Table 2. Comparison of NH_3-sensing performance of the Ag_3PO_4/WO_3 sensor and previously reported sensors.

Material	Gas concentration (ppm)	Operating temperature (°C)	Response (%)	Stability (weeks)	Reference
Single-walled carbon nanotubes	5	50	10	NO	[32]
α-Fe_2O_3-graphene	10	250	13.5	NO	[33]
Cu-WO_3	5	250	100	NO	[34]
Pt-WO_3	10	175	90	5	[35]
WO_3	80	220	95	NO	[36]
Co_3O_4	200	160	153	2	[37]
rh-In_2O_3	5	300	70	NO	[38]
SnO_2-Pd-rGO	5	RT	7.6	10	[39]
ZnO-rGO	50	RT	19.2	18	[40]
In situ double-layer TiO_2 NRAs	50	RT	61	2	[12]
Ag_3PO_4-WO_3	100	RT	70	5	this work

Note: NRAs, nanorod arrays; rGO, reduced graphene oxide.

3.3. Gas-sensing mechanism

The gas-sensing mechanism of the sensor is believed to involve the adsorption of gas molecules on the surface of the semiconductor materials and charge transfer between the surface and the adsorbed molecules, which could eventually produce changes in the electronic configuration and conductivity of the semiconductors.[41] In the present study, the gas-sensing mechanism of Ag_3PO_4/WO_3 sensor comprised two main steps, oxidation and reduction. During oxidation, the adsorbed oxygen molecules on the surface of Ag_3PO_4/WO_3 were converted into oxygen species by trapping electrons from the conduction band of Ag_3PO_4/WO_3. As a result, an electron depletion layer was formed on the surface of the Ag_3PO_4/WO_3 composite. The width of the depletion layer depended upon the number of oxygen species (room temperature for O_2^- species) formed on the surface of Ag_3PO_4/WO_3 as well as the number of available electrons. The depletion layer found on the surface of Ag_3PO_4/WO_3 composites is much thicker than that on pristine Ag_3PO_4 and WO_3 due to the synergistic ef-

fect between Ag_3PO_4 and WO_3, which remarkably narrows the width of the conduction channel of electrons in the composites; this effect was realized by the method of energy band designing.

The synergistic effect of Ag_3PO_4 and WO_3 will now be discussed in detail. The conduction and valence bands of Ag_3PO_4 have a more negative potential (conduction band 0.45 eV, valence band 2.90 eV) than those of WO_3 (conduction band 0.64 eV, valence band 3.34 eV). Therefore, the electrons are transferred from the conduction band of Ag_3PO_4 to the conduction band of WO_3, as shown in Fig. 10(b). At the same time, transport of holes took place from the valence band of WO_3 to the valence band of Ag_3PO_4. Band bending occurred in the energy band and the Fermi level reached equilibrium. Next, a barrier (qV) between Ag_3PO_4 and WO_3 was created, which in turn improved the efficient separation of electron–hole pairs and increased the resistance of the materials (Fig. 10(c)). The relationship between the resistance and barrier height is $R \propto \exp\left(-\frac{qV}{2kT}\right)$, where R is the resistance of the sensor, qV is the barrier height, k is the Boltzmann constant and T is the absolute temperature.[42] The improved separation of electron–hole pairs effectively reduces the number of electrons in the conduction band of Ag_3PO_4, thus avoiding the conversion of silver ions into metallic silver. The synergistic effect realized by energy band designing not only significantly improves the stability of Ag_3PO_4 but also greatly increases the resistance of the materials, further enhancing the sensitivity of the sensor. In addition, rich grain boundaries exist with the adjacent Ag_3PO_4 nanoparticles, Ag_3PO_4 nanoparticles and WO_3 as well as WO_3, leading to abundant trap states and deep defect states; these provide more active sites for the adsorption of molecules and the transport of electrons.[29]

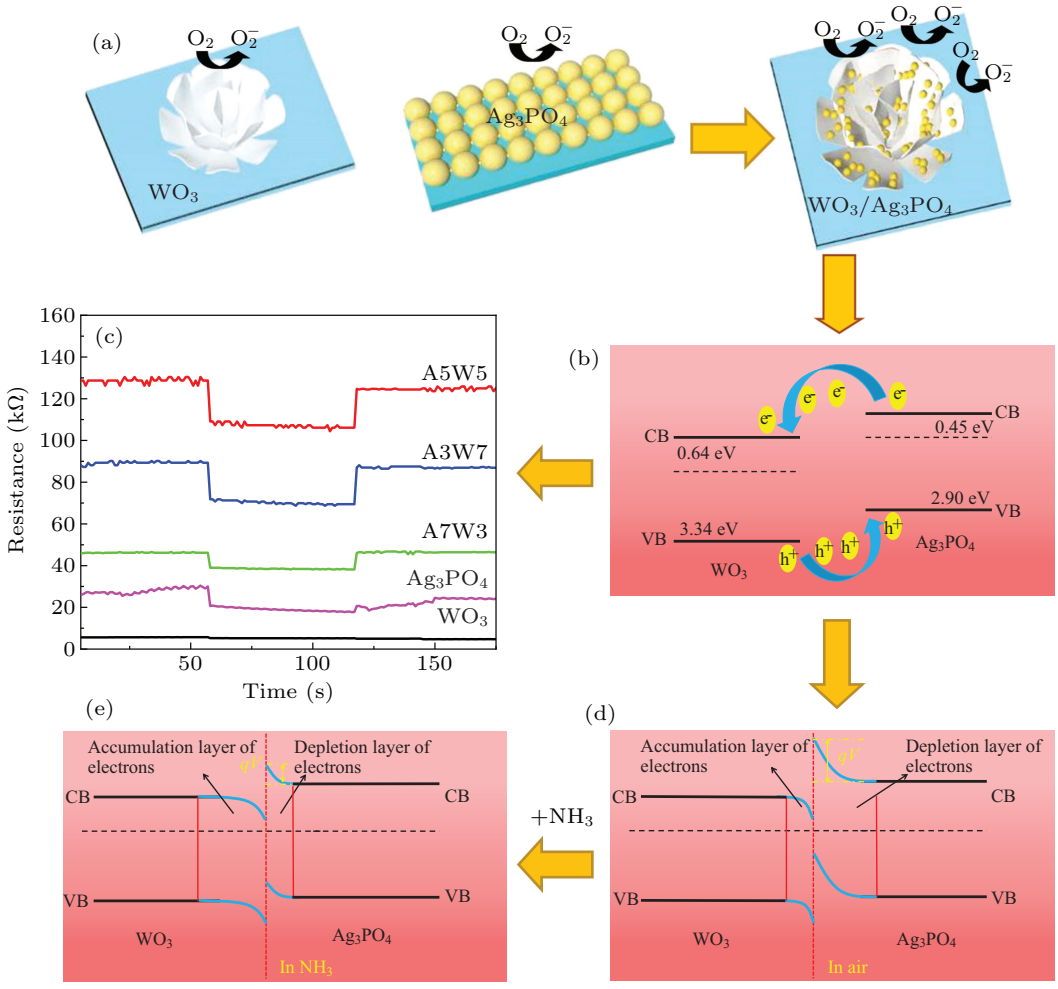


Fig. 10. (a) Diagram of Ag_3PO_4/WO_3 composites. (b), (e), (d) The energy band diagram of the composite. (c) The change in resistance of the materials in 20 ppm NH_3.

The above discussion has sufficiently proved that the gas-sensing performance of composites is much better than that of the single nanomaterials. During reduction, the previously formed O_2^-(ads) interacted with NH_3 molecules to form nitrogen (N_2). This procedure released the trapped electrons back to the conduction band of the composite material. Consequently, the thickness of the accumulation layer was increased whereas the thickness of the depletion layer and the height of the barrier were decreased by the gain of electrons from the oxygen species when NH_3 is injected into the gas chamber (Fig. 10(e)).

In order to better understand the surface reaction process,

attenuated total reflection Fourier transform infrared spectroscopy (ATR-FTIR) was performed; the results are shown in Fig. S4 (NH_3 atmosphere, red line; air atmosphere, black line). The absorption peak located at 1630 cm^{-1} was present in both red and black lines, due to the existence of O–H bonds in the water molecules in the sample.[43,44] However, the peak at 3441 cm^{-1} was only observed in the NH_3 atmosphere, which can be attributed to the stretching vibration of the O–H in the water molecules that were formed by the reaction of NH_3 (ads) and O_2^- (ads).[43,44] The absorption peak of N_2 was not found due to the invariant dipole moment of N_2 molecules. The above process is described in Fig. 10 and the following equations:

$$O_{2(gas)} \rightarrow O_{2(ads)}, \tag{1}$$

$$O_{2(ads)} + e^- \rightarrow O^-_{2(ads)}, \tag{2}$$

$$NH_{3(gas)} \rightarrow NH_{3(ads)}, \tag{3}$$

$$4NH_{3(ads)} + 3O^-_{2(ads)} \rightarrow 2N_2 + 6H_2O + 5e^-. \tag{4}$$

4. Conclusions

In the present study, composites of Ag_3PO_4 nanoparticles and 3D peony-like WO_3 with different mass ratios were successfully prepared by a precipitation method. The gas-sensing performance of the composites to NH_3 was systematically investigated at room temperature. Among the different composite sensors tested in this study, the A5W5 gas sensor displayed the highest response to NH_3 and had excellent selectivity. Interestingly, all the composite gas sensors exhibited a higher response and lower detection limit (1 ppm) to NH_3 than the pure Ag_3PO_4 and WO_3 sensors due to the synergistic effect achieved by the heterojunction structure design. In addition, this method not only enhanced the response of the sensors but also improved the stability of the Ag_3PO_4 sensors to a greater extent. Therefore, the Ag_3PO_4-based sensors developed in this study could be ideal candidates for the detection of NH_3 under extreme environmental conditions.

Acknowledgements

The authors sincerely acknowledge the financial support from the Collaborative Education Project of Industry-University Cooperation of the Ministry of Education of China (Grant No. 202101256024) and the National Natural Science Foundation of China (Grant Nos. 11904209 and 61802144).

References

[1] Wetchakun K, Samerjai T, Tamaekong N, Liewhiran C, Siriwong C, Kruefu V, Wisitsoraat A, Tuantranont A and Phanichphant S 2011 *Sens. Actuators B* **160** 580
[2] Toan N V, Hung C M, Hoa N D, Duy N V, Le D T T, Hoa N T T, Viet N N and Phuoc P H and Hieu N V 2021 *J. Hazard. Mater.* **412** 125181
[3] Wang L, Lou Z, Zhang R, Zhou T, Deng J and Zhang T 2016 *ACS Appl. Mater. Interfaces* **8** 6539
[4] Liu X, Chen N, Han B, Xiao X, Chen G, Djerdj I and Wang Y 2015 *Nanoscale* **7** 14872
[5] Li Y, Ban H and Yang M 2016 *Sens. Actuators B* **224** 449
[6] Moshirian-Farahi S S, Zamani H A and Abedi M R 2022 *Nanotechnology* **33** 195502
[7] Patil L A, Bari A R, Shinde and Deo V 2010 *Sensor Rev.* **30** 290
[8] Shao F, Fan J D, Hernández-Ramírez F, Fàbrega C, Andreu T, Cabot A, Prades J D, López N, Udrea F, De Luca A, Ali S Z and Morante J R 2016 *Sens. Actuators B* **226** 110
[9] Lee J, Lee S H, Bak S Y, Kim Y, Woo K, Lee S, Lim Y and Yi M 2019 *Sensors* **19** 1903
[10] Nikolaev A L, Kazmina M A, Lyanguzov N V, Abdulvakhidov K G and Kaidashev E M 2022 *J. Adv. Diele.* **12** 2160020
[11] Su P G, Chen F Y and Wei C H 2018 *Sens. Actuators B* **254** 1125
[12] Zhao G, Xuan J, Gong Q, Wang L, Ren J, Sun M, Jia F, Yin G and Liu B 2020 *ACS Appl. Mater. Interfaces* **12** 8573
[13] Cui S, Yang L, Wang J and Wang X 2016 *Sens. Actuators B* **233** 337
[14] Lu T, Lv J and Wang C 2022 *J. Alloy. Compd.* **897** 163135
[15] Jeevanandam J, Barhoum A, Chan Y S, Dufresne A and Danquah M K 2018 *Beilstein J. Nanotech.* **9** 1050
[16] Li Z, Liu X, Zhou M, Zhang S, Cao S, Lei G, Lou C and Zhang J 2021 *J. Hazard. Mater.* **415** 125757
[17] Zhang J, Liu X, Neri G and Pinna N 2016 *Adv. Mater.* **28** 795
[18] Huo L, Yang X, Liu Z, Tian X, Qi T, Wang X, Yu K, Sun J and Fan M 2017 *Sens. Actuators B* **244** 694
[19] Liu Z, Yang X, Huo L, Tian X, Qi T, Yang F, Wang X, Yu K, Ma F and Sun J 2017 *Sens. Actuators B* **248** 324
[20] Zhou X, Wang X, Wang B, Chen Z, He C and Wu Y 2014 *Sens. Actuators B* **193** 340
[21] Park M S, Kim K H, Kim M J and Lee YS 2016 *Colloids Surf. A* **490** 104
[22] Yan F, Shen G, Yang X, Qi T, Sun J, Li X and Zhang M 2019 *Appl. Surf. Sci.* **479** 1141
[23] Xiao W, Liu W, Mao X, Zhu H and Wang D 2013 *J. Mater. Chem. A* **1** 1261
[24] Chang Y, Yu K, Zhang C X, Li R, Zhao P Y, Lou L L and Liu S X 2015 *Appl. Catal. B* **176** 363
[25] Li T, Wei H, Jia H, Xia T, Guo X, Wang T and Zhu L 2019 *ACS Sustain. Chem. Eng.* **7** 4177
[26] Tang C, Liu E, Fan J, Hu X, Ma Y and Wan J 2015 *RSC Adv.* **5** 91979
[27] Tao R, Yang S, Shao C, Li X, Li X, Liu S, Zhang J and Liu Y 2019 *ACS Appl. Nano Mater.* **2** 3081 DOI:
[28] Cai G F, Tu J P, Zhou D, Li L, Zhang J H, Wang X L and Gu C D 2014 *CrystEngComm* **16** 6866
[29] Xu Y, Zheng L, Yang C, Liu X and Zhang J 2020 *Sens. Actuators B* **304** 127237
[30] Yang X, Cui H, Li Y, Qin J, Zhang R and Tang H 2013 *ACS Catal.* **3** 363
[31] Kolhe P S, Mutadak P, Maiti N and Sonawane K M 2020 *Sens. Actuators A* **304** 111877
[32] Tsuruta A, Akamatsu T, Naito K, Hirai T, Murase S and Masuda Y 2021 *ECS J. Solid. State. Sc.* **10** 121004
[33] Haridas V, A. Sukhananazerin, Mary Sneha J, Pullithadathil B and Narayanan B 2020 *Appl. Surf. Sci.* **517** 146158
[34] Anusha, Antony A, Ani A, Poornesh P and Kulkarni S D 2021 *Mater Sci. Semicond. Process* **133** 105967
[35] Li T T, Zhou P F, Zhao S K, Han C, Wei D Z and Shen Y B 2021 *Vacuum* **184** 109936
[36] Takács M, Dücső C and Pap A E 2015 *Sens. Actuators B* **221** 281
[37] Deng J, Zhang R, Wang L, Lou Z and Zhang T 2015 *Sens. Actuators B* **209** 449
[38] Jiang H, Zhao L, Gai L, Ma L, Ma Y and Li M 2013 *CrystEngComm* **15** 7003
[39] Su P G and Yang L Y 2016 *Sens. Actuators B* **223** 202
[40] Wang T, Sun Z, Huang D, Yang Z, Ji Q, Hu N, Yin G, He D, Wei H and Zhang Y 2017 *Sens. Actuators B* **252** 284
[41] Shaikh S F, Ghule B G, Nakate U T, Shinde P V, Ekar S U, Dwyer C O, Kim K H and Mane R S 2018 *Sci. Rep.* **8** 1106
[42] Yu Q, Jin R, Zhao L, Wang T, Liu F, Yan X, Wang C, Sun P and Lu G 2021 *ACS Sens.* **6** 3451
[43] Li Z J, Lin Z J, Wang N N, Wang J Q, Liu W, Sun K, Fu Y Q and Wang Z G 2016 *Sens. Actuators B* **235** 222
[44] Srirattanapibul S, Nakarungsee P, Issro C, Tang I M and Thongmee S 2021 *Mater. Chem. Phys* **272** 125033